An Inverse Analysis Procedure for Material Parameter Identification of Mortar Joints in Unreinforced Masonry

C. Chisari[1], L. Macorini[2], C. Amadio[1] and B.A. Izzuddin[2]

[1] Department of Engineering and Architecture, University of Trieste, Piazzale Europa 1, 34127 Trieste, Italy,
[2] Department of Civil and Environmental Engineering, Imperial College London, South Kensington Campus, London SW7 2AZ.

Abstract

Many old unreinforced masonry (URM) structures still in use need to be assessed considering the safety requirements proposed by current codes. Because of the complexity of the URM response, sophisticated numerical descriptions are required for an accurate structural assessment. When inverse analysis is used for the identification of material properties, the study of the effects of measurement errors is essential for assessing the robustness of the adopted procedure. In this work, inverse analysis techniques utilising Genetic Algorithms are employed to calibrate elastic material parameters of an advanced mesoscale model for URM. In order to apply this strategy to in-situ low-invasive investigations, a non-conventional flat-jack test setup is proposed. The potential and limitations of the method are analysed using computer-generated pseudo-experimental data with different noise limits. This allows the evaluation of the influence of the measurement equipment precision on the stability of the inverse problem.

Keywords: Inverse analysis, unreinforced masonry, mesoscale model, genetic algorithms, interface elements, noise analysis.

1. Introduction

Even though in the last century many building techniques have been developed and utilised, most of historical structures all over the world are made up of unreinforced masonry (URM). Buildings, monuments and bridges, some of which are still in use, were often built following rules-of-thumb and trial-and-error procedures but not a sound engineering approach. Thus one of the major problems in modern structural engineering is assessing the safety of these old structures when subjected to the loads prescribed by modern codes. The response of masonry especially under extreme loading (e.g. earthquake) is very complex because of URM inherent heterogeneous nature and nonlinear behaviour. In the recent past significant research

has been devoted to the development of accurate numerical models for the structural assessment of URM structures [1]. Two alternative approaches, namely macro- and mesoscale modelling [2], [3], can be considered for analysing the response of URM components up to collapse. According to the macroscale strategy, URM is represented as a homogeneous continuous material [4]. On the other hand, when using mesoscale modelling, masonry units, mortar and brick-mortar interfaces are modelled separately to account explicitly for the characteristic URM anisotropy due to the specific arrangement of units and mortar joints. To reduce the computational cost, mortar and brick-mortar interfaces can be effectively modelled with zero-thickness interface elements based on plastic [5], [6] or damage mechanics theories [7] to account for material nonlinearity.

In general, when using any modelling strategy, the calibration of material parameters represents a critical process which determines the accuracy of the structural analysis. Macro-modelling material parameters should be obtained from expensive and invasive in-situ tests on masonry panels [8], because they must represent the behaviour of a significant volume of the structure. Conversely, mesoscale modelling adopts material parameters derived directly from simple low-invasive tests on units and mortar. However, while simple tests can provide realistic strength parameters for mortar and bricks, they do not normally enable an accurate estimate for the stiffness of brick-mortar interfaces [3], [9], [10]. Thus specific experimental setups and procedures for experimental data analysis are required to obtain such critical material parameters. In this respect, inverse analysis utilising optimization techniques has been established as an effective and sound procedure for the calibration of model material parameters in a wide range of applications [11], [12]. It may be particularly effective when using complex numerical models, in which the determination (or even the physical meaning) of the material parameters is not straightforward. In general, while a direct structural analysis uses “input” parameters (material parameters, loads, etc.) to obtain “output” variables (displacements, strains and stresses), an inverse analysis aims to determine “input” values from the observation of the structural response. The inverse problem is generally solved through the use of an optimization approach, in which a discrepancy function between the computed output variables (given a trial set of input parameters) and the measured entities is minimised. While calibration methods with dynamic tests and inverse analysis techniques (dynamic inverse analysis) are now well-established for determining constitutive elastic parameters of existing structures [13], [14], [15], the use of static tests may represent a more suitable and cheaper strategy when nonlinear material parameters are to be sought [16]. However, the results obtained by applying inverse analysis with experimental static tests (static inverse analysis) may be less accurate, mainly because of the limited amount of information that static tests can supply [17]. Thus, in static inverse analysis, the assessment of the noise effects on the parameter estimation (noise analysis) is critical. This is discussed in [18], where the influence of the number of sensors and their location on the accuracy of the solution in a soil-structure interaction parameter identification inverse problem is investigated.

In this work, inverse analysis procedures with Genetic Algorithms (GA) [19], [20] are applied to the calibration of the main elastic parameters of an advanced

mesoscale model for URM [6]. To this end, a flat-jack test setup to be used in low-invasive experimental tests is considered. This was investigated by the authors in [21], where a pseudo-experimental approach was followed by replacing the experimental data with numerical results obtained using specific material input parameters. This study is herein extended considering the influence of the number and position of different displacement measures. In particular, a sensitivity analysis in the neighbourhood of the solution has been carried out, while a noise analysis has been performed to estimate the stability of the procedure. Moreover a fixed-range random error has been introduced to account for the limited precision of the measurement equipment used in the experimental test.

2. Overview of the calibration problem

Let Θ be a physical system; the procedure for studying Θ typically involves two steps which are intrinsically bound: i) parameterisation, that is, choosing a minimal set $\boldsymbol{x}$ of *model parameters*, and ii) *forward modelling*, i.e. definition of the physical laws which allow us, for given values of the model parameters, to predict the system response, i.e. the values of some *observable variables*.
In particular, for structural problems, the model (or material) parameters $\boldsymbol{x}$ can be associated with quantities (strains, stresses, displacements, reactions) $\boldsymbol{y}$ through the relationship:

$$\boldsymbol{y} = H(\boldsymbol{x}) \tag{1}$$

where $H(\boldsymbol{x})$ is a function usually called *forward operator*. Defining such mathematical operator is essential for the study of a structural system and it can be represented by an analytical formulation or a specific finite element (FE) model. Clearly, the choice of the *forward operator* is rather arbitrary, since the same physical phenomenon can be represented by different (more or less complicated) models, which involve different parameters. In any case, special care has to be taken to guarantee that H can effectively represent the overall response.
Equation (1) represents a nonlinear system in the unknowns $\boldsymbol{x}$, when the response $\boldsymbol{y}$ (collected in a vector of size L) is known. Clearly, the exact response is represented by the complete independent scalar/vector/tensor fields which control the model itself. In the case of FE models, the complete displacement field of the structure univocally determines the response, because, once it is known, strains, stresses and reactions can be evaluated using compatibility, constitutive laws and equilibrium. In this respect, two problems arise: i) invertibility of (1) is not always assured, ii) it is usually not possible to record an entire displacement field in experimental tests, where only a limited set of values can be monitored.
Therefore, the problem (1) is replaced by:

$$\boldsymbol{x} = {H_r}^{-1}(\boldsymbol{y^m}) \tag{2}$$

in which $\boldsymbol{y^m}$ is the N-sized vector of measured quantities (with N number of measurements and $N < L$) and $H_r(\boldsymbol{x})$ is the corresponding reduced subset of the

complete system. The choice of $\boldsymbol{y^m}$ is crucial, since it can lead to an ill-posed "reduced" inverse problem (2), even when system (1) is solvable.
When a complex FE model is used, the function $H_r(\boldsymbol{x})$ is not known as a simple mathematical formulation. This is not explicitly invertible, thus numerical procedures are required to solve (2). A possibility is represented by the minimization of the discrepancy function $\omega(\boldsymbol{x})$:

$$\omega(\boldsymbol{x}) = \boldsymbol{R^T W R} \tag{3}$$

with $\boldsymbol{R} = \boldsymbol{y^c}(\boldsymbol{x}) - \boldsymbol{y^m}$ being the residual vector between the measured displacements y^m_i, with i = 1, …, N and the computed displacements y^c_i, that are obtained for a chosen set of trial parameters $\boldsymbol{x}$. $\boldsymbol{W}$ is a weight matrix that accounts for the correlation between response variables and is usually chosen as the inverse of the covariance matrix [22]. Alternatively, $\boldsymbol{W}$ can be assumed as a diagonal matrix which assigns to each component of the residual vector $\boldsymbol{R}$ a weight inversely proportional to the corresponding measurement scattering. This is needed when different types of measures are available (reactions, displacements), and in general when different precision levels are to be expected in the measurements. Moreover, it is important to point out that $\boldsymbol{W}$ is another factor that strongly influences the possibility to reach the solution, because it significantly changes the discrepancy function.
As stated, a careful choice of the subset $H_r(\boldsymbol{x})$ is needed. Let us suppose that $H_r(\boldsymbol{x})$ can be assumed differentiable in an open ball B around $\boldsymbol{x^r}$, where $\boldsymbol{x^r}$ is the solution of (1) and consequently of (2). With such hypothesis, the reduced forward operator can be approximated by Taylor's series to the first derivative:

$$y_j \cong y_j^{\boldsymbol{m}} + \sum_{i=1}^{M} \left.\frac{\partial y_j}{\partial x_i}\right|_{\boldsymbol{x}=\boldsymbol{x^r}} \cdot (x_i - x_i^r) \qquad j = 1, \dots, N \tag{4}$$

with M the dimension of the $\boldsymbol{x}$ vector.
Imposing a change of variables: $\widetilde{y_j} = 1 - \frac{y_j}{y_j^{\boldsymbol{m}}}$ and $\widetilde{x_i} = 1 - \frac{x_i}{x_i^r}$, Equation (4) becomes:

$$\widetilde{y_j} \cong \sum_{i=1}^{M} S_{ij}\, \widetilde{x_i} \tag{5}$$

with:

$$S_{ij} = \left.\frac{\partial y_j}{\partial x_i}\right|_{\boldsymbol{x}=\boldsymbol{x^r}} \cdot \frac{x_i^r}{y_j^m} \tag{6}$$

where S_{ij} is a component of the sensitivity matrix $\boldsymbol{S}$ and corresponds to the sensitivity index of the measurable variable y_j with respect to the input variable x_i. By transforming a nonlinear system into a local linear one, the analysis of the sensitivity matrix $\boldsymbol{S}$ can provide some insights into the solution.
Let us consider the (possibly) over-determined system

$$\boldsymbol{Ax} = \boldsymbol{b} \tag{7}$$

where the matrix $\boldsymbol{A} \in \mathbb{R}^{N\times M}$ and $N \geq M$ with full column rank, e.g. *rank(**A**)=M*. The general definition for the *relative normwise condition number* κ when the errors appear in the right-hand term is [23]:

$$\kappa(\boldsymbol{A}, \boldsymbol{b}) = \lim_{\varepsilon\to 0} \sup_{\|\boldsymbol{\Delta b}\|\leq\varepsilon} \left(\frac{\|\boldsymbol{\Delta x}\|}{\|\boldsymbol{x}\|} \Big/ \frac{\|\boldsymbol{\Delta b}\|}{\|\boldsymbol{b}\|} \right) \tag{8}$$

where $\boldsymbol{x}$ is the solution of (7), $\boldsymbol{\Delta b}$ is a perturbation on the right-hand term, $\boldsymbol{\Delta x}$ is the corresponding perturbation in the solution and $\|\cdot\|$ is a suitable norm. κ is a measure of the worst-case sensitivity of the output data to small perturbation to input data and provides an upper bound to the propagation of the error. The condition number in the 2-norm is defined by:

$$\kappa(\boldsymbol{A}, \boldsymbol{b}) = \kappa(\boldsymbol{A}) = \frac{\sigma_{max}}{\sigma_{min}} \tag{9}$$

where σ_{max} and σ_{min} are the maximal and the minimal singular values of matrix $\boldsymbol{A}$.
A qualitative comparison among different measurement data for the discrepancy function (3) can be carried out investigating the stability of the local system (5) through the use of the condition number $\kappa(\boldsymbol{S})$. Large condition numbers are indicators of a significant propagation of errors and so of an ill-conditioned problem.

3. The optimization tool

As discussed in Section 2, a numerical iterative process minimizing the discrepancy function (3) is required to solve the inverse problem in (2). Since assessing the global convexity of $\omega(\boldsymbol{x})$ is not possible, metaheuristics as Evolutionary Strategies [24], Simulated Annealing [25] or Genetic Algorithms (GA) [19], [20] can be effectively employed.
In this work, a GA procedure has been used. The main idea is to let a *population* of several candidate solutions evolve instead of studying only one as required by gradient-based optimization techniques. The first step of the procedure consists of the *chromosome* definition for the problem under study, and the correct representation for it. The chromosome collects the parameters varied during the process: in the problem defined in Section 2 it represents the vector $\boldsymbol{x}$. Each parameter x_i (called *gene*) is represented by a double-precision decimal varying between a lower and upper bound. While the genotypic representation of the genes is called chromosome, each phenotypic instance is an *individual*, and a population is a collection of different individuals.
The initial population can be generated randomly or with pseudo-random techniques. In this work, a Sobol sequence [26] has been used, which allows for a more uniform exploration of the solution space than a simply random generation (Figure 1).

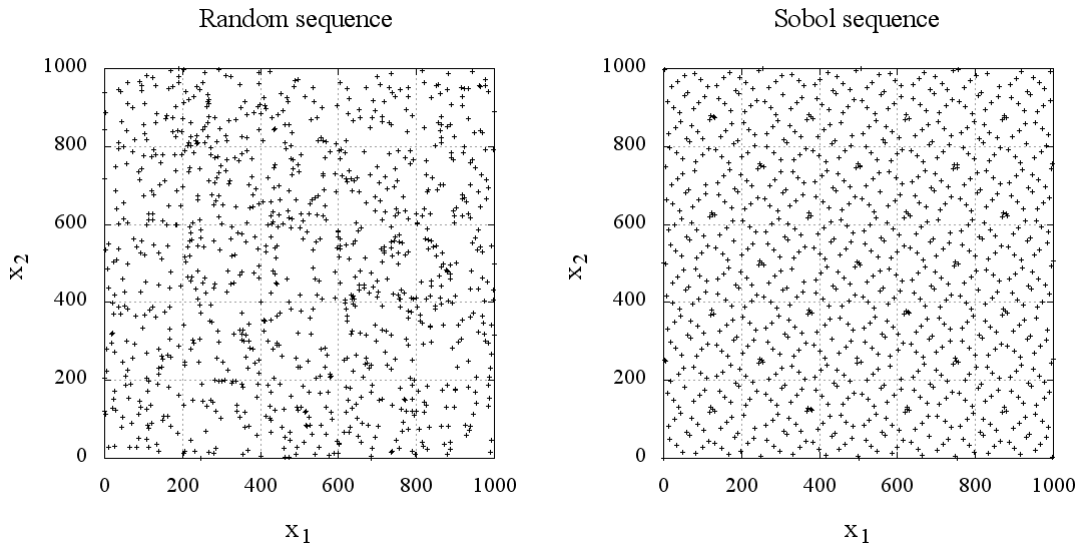


Figure 1. Random (left) and Sobol (right) sequence of 1000 elements in a 2D space

Processing a generation consists of evaluating the discrepancy value (3) (*fitness* in the GA jargon) for each individual. After that, they are ranked based on their fitness. Ranking is not mandatory in the GA, but associated with some particular *selection* schemes it can overcome potential problems like premature convergence. Here, linear ranking is used, according to which a probability linearly proportional to the rank is given to the individual. According to this probability an intermediate population is created, in which the most performing individuals can be duplicated by means of the Stochastic Universal Sampling [27]. This way, their genetic material will be more represented in the next generation. It is possible to calibrate the scaling pressure, i.e. the proportional factor used in the scaling procedure. A scaling pressure equal to 1.0 means that all individuals have the same probability, thus no real scaling is applied. A maximum scaling pressure equal to 2.0 assigns zero probability to survive to the worst individual and twice the average probability to the best individual in the intermediate population.

With the selection, no different individuals are created, but the previous population is rearranged in such a way that the most promising individuals are cloned and the worst deleted. Now, a new generation can be created: given two parents p_1 and p_2, two offspring c_1, c_2 are generated through application of the crossover (or recombination) operator, with a probability p_c. A variant of Arithmetical Crossover [28] is used: the i-th gene h_i^k for the k-th offspring (k = 1, 2) is generated according to the expressions:

$$\begin{aligned} h_i^1 &= \lambda s_i^1 + (1-\lambda) s_i^2 \\ h_i^2 &= \lambda s_i^2 + (1-\lambda) s_i^1 \end{aligned} \qquad (10)$$

where s_i^1, s_i^2 are the i-th gene of the first and the second parent, and $\lambda = \frac{1+\alpha-2\alpha\beta}{2}$. In the expression for λ, α is an interval parameter (chosen by the user), while β is a random number in the interval (0, 1).

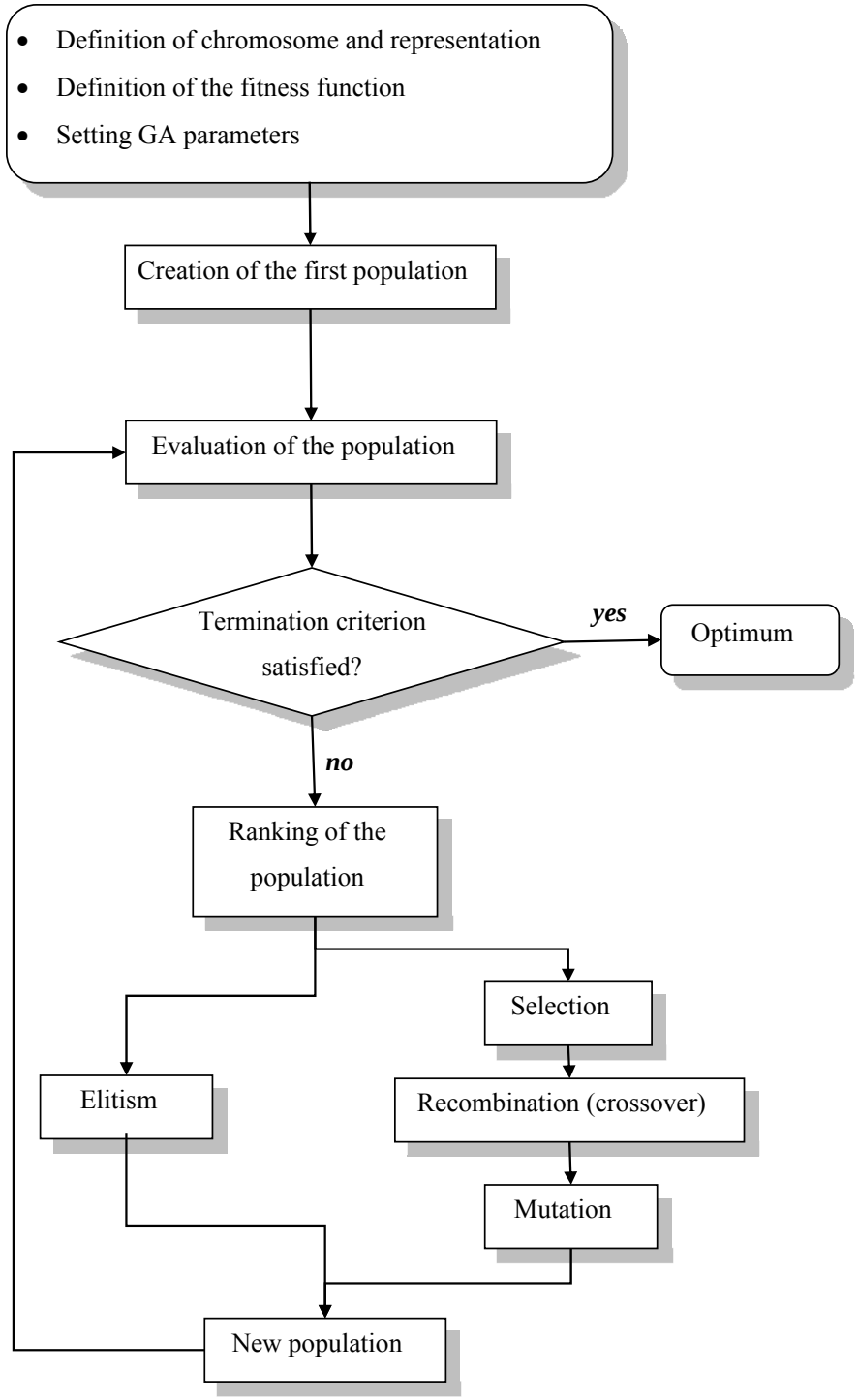


Figure 2. Flow chart of the Genetic Algorithm

In order to improve convergence, an elitist approach has been used [29], in which the best individual among parents and offspring is always placed (without passing through the recombination operator) in the subsequent generation.

Once the new population has been created, mutation is applied to some individuals according to a probability p_m. Mutation is useful to prevent the loss of diversity of

the population, but it is highly disrupting with respect to convergence. For this reason, special care must be taken in the choice of both the type and probability of mutation. In this work a special mutation operator is applied, in which a random gene is modified (as in usual aleatory mutation) but only in the neighbourhood of the individual selected. It means that the mutated gene can assume values inside a small subset of the global variation range, instead of the all range. Thus, in the later generations a lot of individuals are available near the best, increasing the probability to find the real solution. The procedure discussed before is schematically shown in Figure 2.

The process continues with the evaluation of the created generation. From one generation to the next, the most promising genetic material spreads, and the population tends to include only individuals with good fitness. Termination criteria are needed to end the process. Usually the process can be stopped when i) a given maximum number of generations has been formed, ii) a minimum fitness standard deviation in the current population is reached, or iii) a maximum number of generations in which the solution has not been improved has been formed.

4. Mesoscale model for URM

The calibration procedure described in Section 2 combined with the optimization tool detailed in Section 3, has been applied for determining elastic material parameters of an advanced mesoscale description for URM. In this model, mortar and brick–mortar interfaces are modelled by 16-noded nonlinear interface elements [6]. Masonry units are represented by 20-noded continuous elastic elements, and possible unit failure in tension and shear is accounted for by means of zero-thickness interface elements in the vertical mid-plane of all blocks (Figure 3).

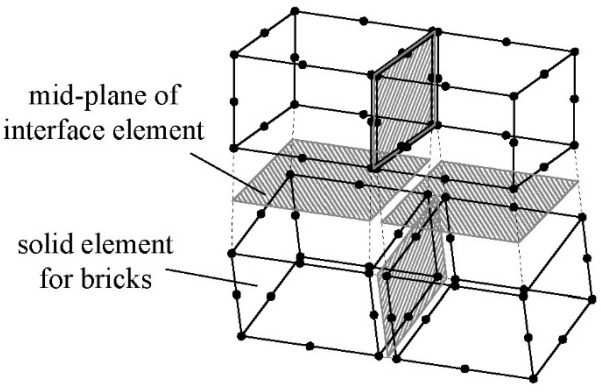


Figure 3. 3D meso-scale modelling for URM with 20-noded solid elements and 2D 16-noded nonlinear interface elements [6].

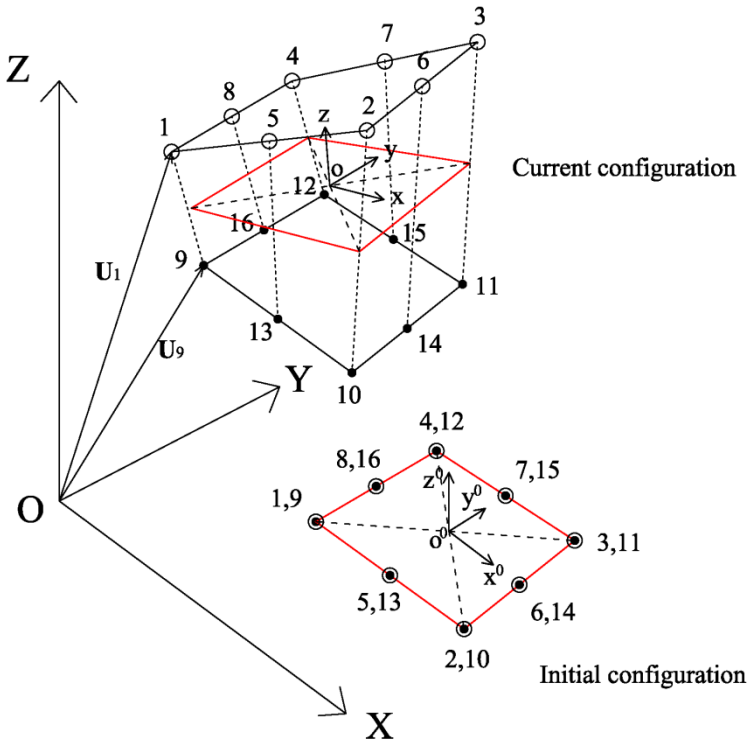


Figure 4. Interface mid-plane in the initial and deformed configuration [6].

This allows for any 3D arrangement of URM to be represented taking into account both initial and damage-induced anisotropy [6]. The interface local material model is formulated in terms of one normal and two tangential stresses **σ** (11) and relative displacements **u** (12) evaluated at each integration point over the reference mid-plane (Figure 4).

$$\boldsymbol{\sigma} = \{\tau_x, \tau_y, \sigma\}^T \tag{11}$$

$$\boldsymbol{u} = \{u_x, u_y, u_z\}^T \tag{12}$$

The constitutive model for zero-thickness interfaces considers specific elastic stiffness values which are regarded as uncoupled:

$$\boldsymbol{k_0} = \begin{bmatrix} k_V & 0 & 0 \\ 0 & k_V & 0 \\ 0 & 0 & k_N \end{bmatrix} \tag{13}$$

In (13), k_N and k_V are respectively the normal and the tangential stiffness, the latter assumed equal in all directions in the local plane *xy*. When applying the mesoscale description to investigate the response of existing URM components, the parameters for masonry units can be easily obtained in simple mechanical tests on small cylindrical specimens which can be extracted in-situ. Conversely, the determination of the mechanical properties for nonlinear interfaces representing mortar joints is more problematic. Particularly difficult is the calculation of the elastic stiffness parameters (13). Analytical expressions for interface stiffness are provided in [2], [3]

as functions of elastic and geometric properties of units and mortar joints. These read:

$$k_N = \frac{E_u E_m}{h_m(E_u - E_m)} \quad k_V = \frac{G_u G_m}{h_m(G_u - G_m)} \tag{14}$$

where E_u, E_m are Young modulus of units and mortar, G_u, G_m are shear modulus of unit and mortar, and h_m is the mortar joint height. The relationships (14), though simple and theoretically founded, may significantly overestimate elastic stiffness of mortar joints. This has been pointed out in [3], where was proposed to reduce the elastic stiffness calculated using (14) to correctly represent the response of real URM panels. Similar stiffness reduction is recommended in [9], while in [10] a correction factor calculated using the results of laboratory experimental tests is proposed and used in mesoscale analysis of URM panel under in-plane loading.
In the following sections, a novel procedure based on inverse analysis of a low-invasive in-situ experimental test setup is described. This allows for an accurate estimation of interface stiffness values for mortar joints.

5. The flat-jack test

An experimental setup has been investigated and used in the calibration procedure for determining the elastic stiffness parameters k_N and k_V. The proposed setup has been designed for low-invasive in-situ experimental static tests on existing structures. In the test, flat-jacks are utilised to apply a specific stress state within a masonry pier. The use of single or double flat-jack is a common procedure for testing existing masonry under compression [30] and shear [31]. Two parallel flat-jacks are usually employed for generating a uniform compressive stress state in a portion of a masonry panel, while the displacement field within the panel is monitored using simple transducers.
The proposed experimental setup consists of a non-conventional shear test, as two flat-jacks are used to apply a controlled pressure along the vertical and horizontal direction (Figure 5). After cutting the masonry panel horizontally (phase 1), a horizontal flat-jack is placed to apply a known compressive stress (phase 2), like in a standard single flat-jack test [30], but not necessarily up to balance the stress originated by the self-weight of the structure above the cut. Afterward, the pressure in the horizontal flat-jack is maintained constant, while the lateral faces of the masonry panel are restrained to prevent any horizontal displacements (Figure 5). Two vertical cuts of equal length are then executed in the area underneath the horizontal flat-jack and a vertical flat-jack is placed in either vertical cut (right cut in Figure 5). Thus an approximately square panel can be tested under shear by increasing the pressure in the vertical flat-jack (phase 3) which gives rise to a displacement field within the panel where the empty cut (vertical cut in Figure 5) is closing.

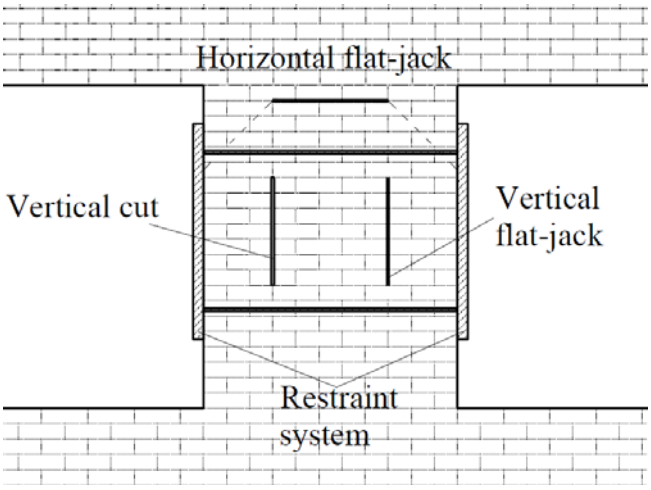


Figure 5. Schematic diagram of the proposed test setup

Clearly, this setup is suitable when it is possible to apply precise boundary conditions to the edges of the tested panel (i.e. when, thanks to the openings, it is possible to apply a restraint system as in Figure 5). When this is not the case, supplementary unknowns representing the panel stress state have to be considered, leading to a problem similar to that discussed in [32], where inverse analysis is applied to investigate mechanical properties of an existing concrete dam.
According to proposed strategy, displacement measurements are considered in the inverse analysis. Their selection is crucial for the definition of the discrepancy function (3). As mentioned in Section 2, as necessary condition for a well-posed problem, the sensitivity matrix **S** in (5) corresponding to the measurements must give a sufficiently small condition number. Furthermore, the measurements have to vary "considerably" in the range of expected values for **y**. This means that the measure instrumentation must have a sufficient sensitivity for the expected measurements and measure variations. In the following, the use of different arrangements for measurement instrumentation is studied and, considering the effects of error propagation, the best measurement equipment and position is identified.

6. Numerical application

The proposed experimental setup has been studied using a pseudo-experimental approach, in which measures $\boldsymbol{y}^{\boldsymbol{m}}$ are generated by a numerical model, with a known set of parameters $\boldsymbol{x}^{\boldsymbol{r}}$. Then the inverse analysis is applied to calculate $\boldsymbol{x}$ from $\boldsymbol{y}^{\boldsymbol{m}}$ and the results are compared against the known $\boldsymbol{x}^{\boldsymbol{r}}$ values. As the same FE model is used for the generation of $\boldsymbol{y}^{\boldsymbol{m}}$ and the minimization of $\omega(\boldsymbol{x})$, model errors are implicitly ruled out.
In the following, the characteristics of the analysed masonry panel are presented, the coefficients for the sensitivity matrix are provided and the stability of the local system (5) is studied, allowing for some preliminary considerations about the

propagation of measurement errors. Finally a noise analysis is performed to experimentally investigate the influence of measurement errors on the sought parameters.

6.1. Model properties

The analysed masonry component is a running bond masonry pier, which has b = 900 mm width, h = 1425 mm height and 102.5 mm thickness. It is made up with 215 × 102.5 × 65 mm^3 bricks and 10 mm thickness mortar joints. In the numerical simulations, the URM panel shown in Figure 6 is analysed using the mesoscale approach proposed in [6] and implemented into ADAPTIC [33] a general Finite Element code developed at Imperial College London. According to the mesoscale description, two solid elements are used for each brick while zero-thickness interface elements model mortar joints. Concerning the properties for the component materials, an elastic modulus E_b = 2500 MPa and Poisson's ratio ν_b = 0.2 have been considered for bricks, while elastic stiffness k_N = 48 N/mm^3 and k_V = 21 N/mm^3 have been assumed for mortar joints. The latter values correspond to the set of $\boldsymbol{x}^r$ parameters (i.e. the known solution of the calibration problem).
The nodes respectively on the right and left edges have been coupled by means of elastic springs, the stiffness of which has been assumed equal to 105560 N/mm. This is equivalent to a restraint system formed by 4Ø12.
In the numerical simulation, it is not necessary to model self-weight (a priori unknown in existing structures), because the elastic regime allows for the superposition of effects, and so the experimental measurements may refer only to the loads applied by means of the flat-jacks. It means that the only phases modelled are phase 2 and 3. At both the horizontal and vertical cuts (Figure 6), a uniform pressure p = 0.3 MPa is applied. The intensity of the pressure has been selected to maintain the structure elastic, while giving rise to displacements large enough to be measured by typical extensometers. In Figure 7, the deformed shape of the URM panel modelled using the mesoscale description after the application of the horizontal flat-jack load (phase 2) and the vertical flat-jack loads (phase 3) is displayed. The figures have been created using the software GMSH [34] as post-processing tool.

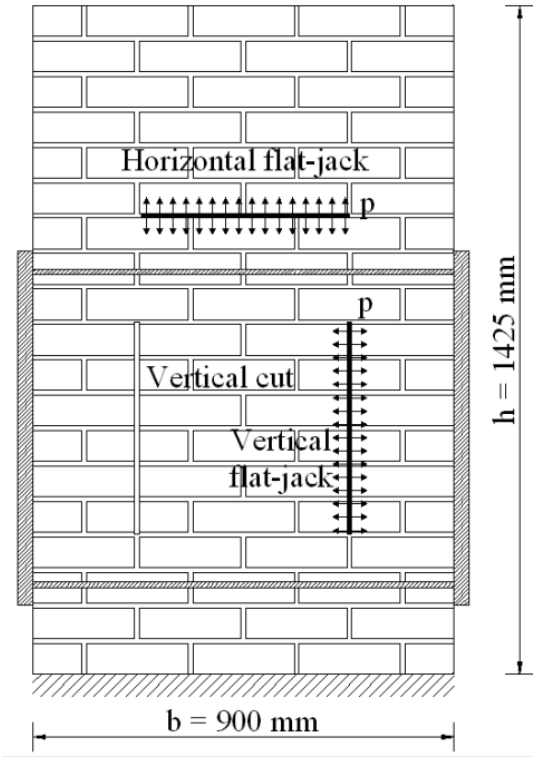


Figure 6. Analysed panel with restraining system and applied loading.

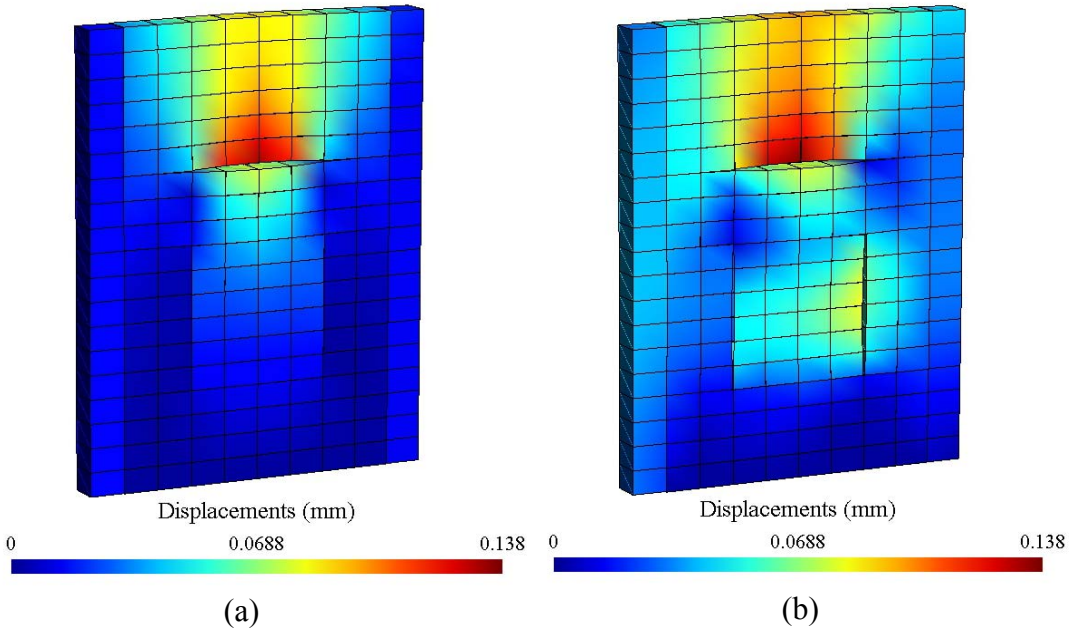


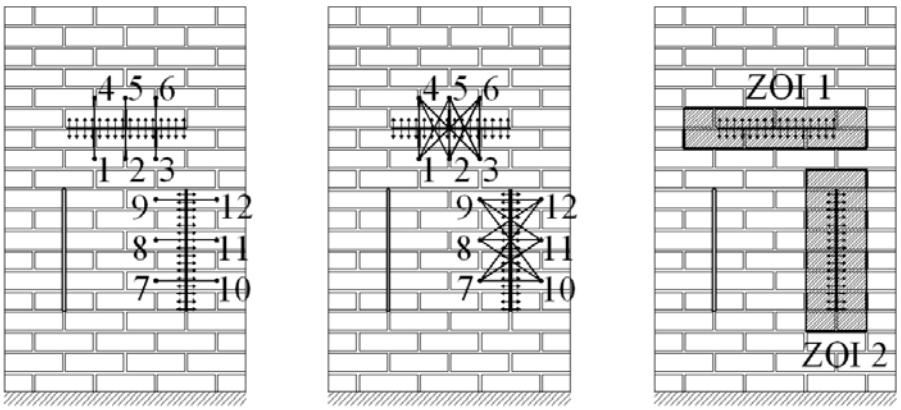
Figure 7. Deformed shape and displacement contour at the end of phase 2 (a) and phase 3 (b)

6.2. The Genetic Algorithm

The Genetic Algorithm described in Section 3 has been used in the calibration procedure. For each sought parameter k_V and k_N which form the chromosome, a lower and an upper bound, equal to 0.45 and 1.6 times the known values, have been considered. The initial population consists of 50 individuals, generated by Sobol sequence, while only 15 individuals have been considered for the subsequent generations to achieve a faster convergence to the solution. The other parameters employed in the GA analyses are: crossover probability $p_c = 1$; crossover parameter $\alpha = 2$; mutation probability $p_m = 0.2$; scaling pressure for linear ranking $p_m = 1.7$; local mutation range over total range ratio: 0.08. The termination criterion is the maximum number of generation. In this respect, it has been observed that 20 generations are usually sufficient to reduce the initial fitness standard deviation by about four orders of magnitude, which guarantees the convergence to the solution.

6.3. The measurements

With the aim of assessing the best measurements for the stability of the procedure, three arrangements have been investigated: (a) 6 extensometers, (b) 18 extensometers, (c) Digital Image Correlation (DIC) [35] for monitoring the continuous displacement field. DIC is an optical method that employs tracking and image registration techniques for accurate 2D and 3D measurements. The comparison between photographs over a zone of interest (ZOI) before and after the application of the load allows for the displacement field to be recorded and displayed.



(a) (b) (c)

Figure 8. Different measurements

In particular, 12 points have been considered as measurement bases for (a) and (b), 6 around the horizontal cut and 6 around the vertical cut (Figure 8). While in the case (a) only relative displacements orthogonal to the cuts are taken into account, in (b) relative displacements also along skew directions are considered. Finally, the areas around the two cuts have been chosen as ZOIs for the application of DIC as

shown in Figure 8c. The measurements at points 1-6 and ZOI 1 are taken after phase 2, while the ones at points 7-12 and ZOI 2 are taken after phase 3.

6.4. Sensitivity analysis

A sensitivity analysis on the measured displacements **y** defined in Figure 8 has been carried out in the neighbourhood of the known solution considering the input parameters ***x***. In the following, both ***x*** and ***y*** have been normalized with respect to the values assumed in the pseudo-experimental analysis. In finite terms, the coefficients of the sensitivity matrix in (6) can be expressed as:

$$S_{ij} \cong \frac{y_j(x_1^r, \dots, x_i^r + \Delta x_i^r, \dots) - y_j(x_1^r, \dots, x_i^r - \Delta x_i^r, \dots)}{2\Delta x_i^r} \cdot \frac{x_i^r}{y_j^m} \qquad (15)$$

where the increments have been taken as $\Delta x_i^r = 10^{-2} \cdot x_i^r$.

Six extensometers

In Table 1 the coefficients of the sensitivity matrix for the test with 6 displacement measurements computed according to (15) are reported. The sensitivity matrix gives a qualitative understanding of which sought parameters significantly influence the measured displacements. It can been seen that the relative displacements Δu_1, Δu_2 and Δu_3, which indicates the opening of the horizontal cut subjected to the vertical pressure *p*, are more dependent on the normal interface stiffness than the shear stiffness. On the other hand, displacements Δu_4, Δu_5 and Δu_6, which are related to the vertical cut opening, are more influenced by the shear stiffness, as expected. Concerning the necessary condition expressed by the local linear system (5), it can be easily found that the matrix **S** has rank 2, while the condition number evaluated by (9) is equal to 7.06.

	Δu_1	Δu_2	Δu_3	Δu_4	Δu_5	Δu_6
k_V	-0.1632	-0.1704	-0.1733	-0.2054	-0.2072	-0.2292
k_N	-0.2388	-0.2329	-0.2387	-0.1949	-0.1814	-0.1516

Table 1. Coefficients for sensitivity matrix **S**

$k_{V,adim}$	$k_{N,adim}$	Δu_1 (mm)	Δu_2 (mm)	Δu_3 (mm)	Δu_4 (mm)	Δu_5 (mm)	Δu_6 (mm)
0.45	1	0.18840	0.22732	0.19417	0.18860	0.22335	0.11175
1.6	1	0.15013	0.17937	0.15301	0.14064	0.16618	0.08090
1	0.45	0.20283	0.24179	0.20755	0.18668	0.21791	0.10383
1	1.6	0.14543	0.17473	0.14893	0.14128	0.16803	0.08362
Pseudo-exp. value (mm)		0.16048	0.19232	0.16438	0.15286	0.18077	0.08891

Table 2. Absolute sensitivity analysis

Moreover, to assess the importance of each sought parameter in absolute terms, extensometer measurements have been evaluated for the extreme values of the

parameter range. The results of this analysis are presented in Table 2, where the pseudo-experimental displacements are compared against the extreme values.
It can be seen that, in general, a considerable variation in the output response is expected when input parameters are varied in their range.

Eighteen extensometers
The same observations reported in the previous subsection are valid here. Again the displacements due to the horizontal flat-jack depend more on k_N, while the ones around the vertical cut are mainly related to k_V. The condition number is very similar to the condition number for the test with 6 extensometers and equal to 7.26.

Digital Image Correlation
The DIC output is a 2D continuous displacement field, so the horizontal and vertical displacement components for each node in the ZOI are recorded. The condition number for the sensitivity matrix obtained considering the variations of all these outputs is equal to 5.11.

6.5. The inverse analysis and random noise

In the final step of the calibration process before performing the inverse analysis, a specific discrepancy function $\omega(\boldsymbol{x})$ has to be defined. This includes the choice of the measurements $\boldsymbol{y}$ and the weight matrix $\boldsymbol{W}$. Referring to the discussion in the previous section, three different choices have been considered for $\boldsymbol{y}$, while an identity matrix was utilised for $\boldsymbol{W}$, as the measurements considered in the procedure are uniform.
In real tests, the measured variables $\boldsymbol{y^m}$ are always affected by some errors because of the limited accuracy of the measurement device. So, it is important to verify the stability of the solution when random errors affect $\mathbf{y}$. In this numerical example, four error ranges have been considered: ±0.5%, ±1%, ±2%, ±5%. For each range, 30 uniformly random series of errors measurements Δu_i are generated. So, for each error range 30 sets of pseudo-experimental values have been assumed to represent $\boldsymbol{y_m}$ in Equation (3). The inverse analysis has been then performed for each perturbed set of measurement values. The dispersion in the results, namely in the sought parameters k_V and k_N, shows the stability of the procedure with respect to the precision of the measurements. These results are displayed in Figure 9-11.

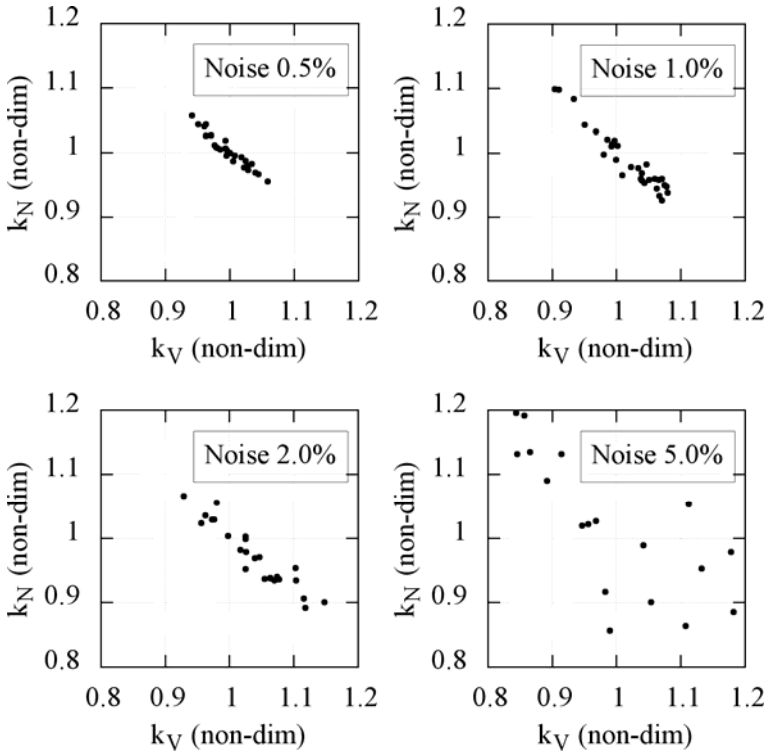


Figure 9. Noise analysis for 6 extensometers

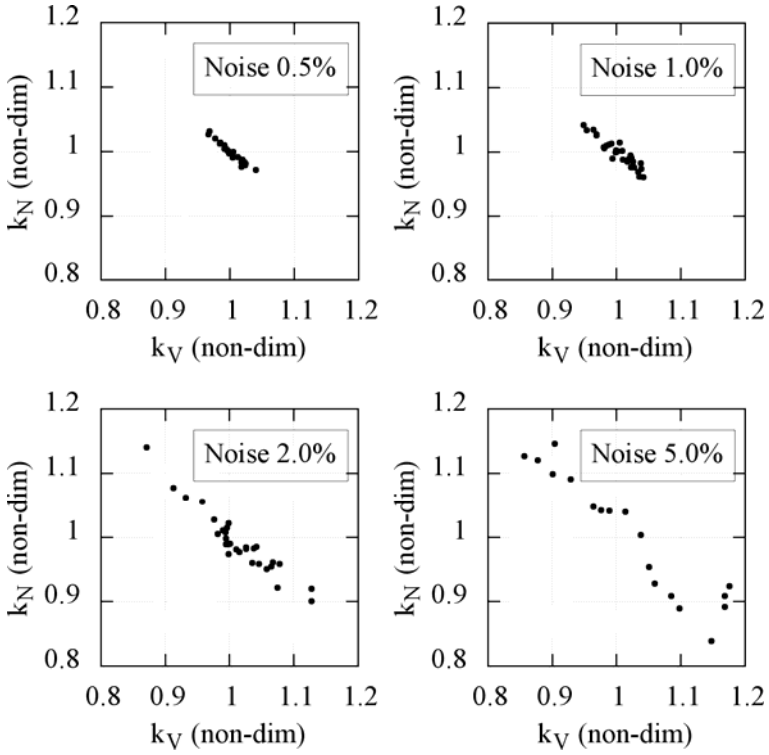


Figure 10. Noise analysis for 18 extensometers

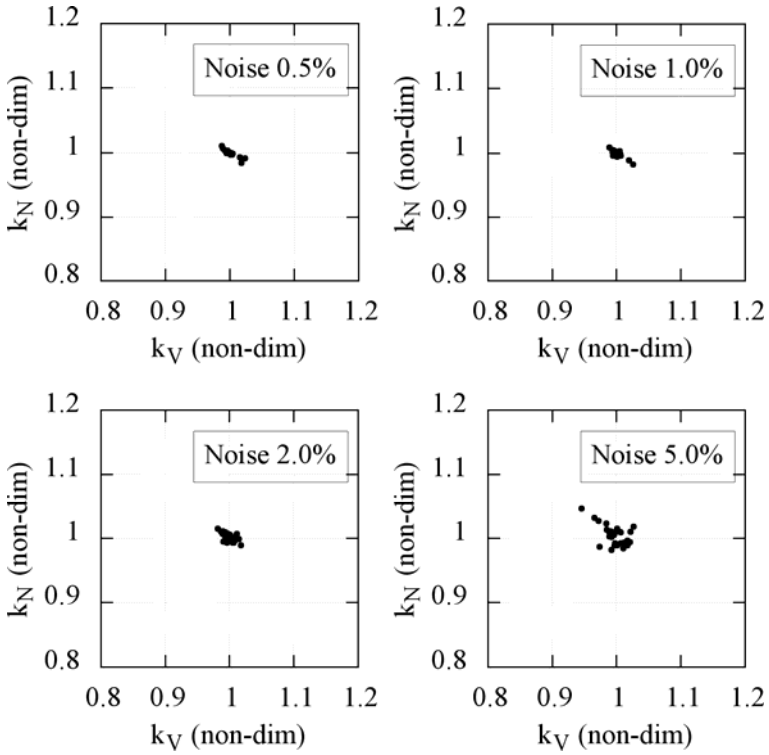


Figure 11. Noise analysis for DIC

It has been seen in Section 6.3 that the three options analyzed have comparable and quite low condition numbers. Thus it is expected that at least in the proximity of the real solution (where linear approximation (5) can be considered valid), the inverse problem is stable, i.e. small perturbations in the measurements induce small errors in the solution. It is confirmed by the numerical tests performed with a random error in the ±0.5% range in all cases.

An interesting trend can be noticed in the Figures 9, 10 and 11. A uniform perturbation of the measurements does not affect the parameter identification in a uniform way. Especially in the case where 6 and 18 measurements are used and for error ranges up to ±2%, the elastic stiffnesses are distributed along a preferential axis with negative slope in the k_V-k_N plane. So, it can be useful to compare parameter distribution considering the variance-covariance matrix, and perform an eigenvalue analysis to find the maximum variance σ_{max}^2. Its square root σ_{max} is proportional to the maximal semi-axis of the covariance ellipse (Figure 12). In Figure 12 an example of 2.0σ covariance ellipse is shown, that is the ellipse in which the axes are scaled so that their semi-length is equal to 2.0σ. In the case of normal distribution, this corresponds to a confidence interval of 95%.

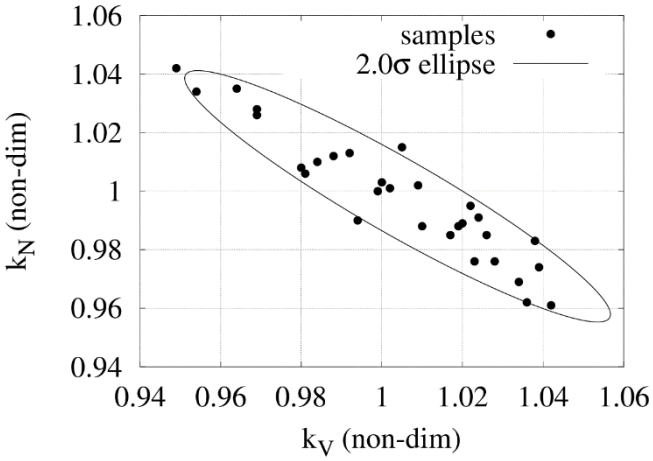


Figure 12. 2.0σ covariance ellipse for the samples with 1.0% error range and 18 extensometers

Using σ_{max} it is possible to compare the three studied measurement arrangements as shown in Figure 13.

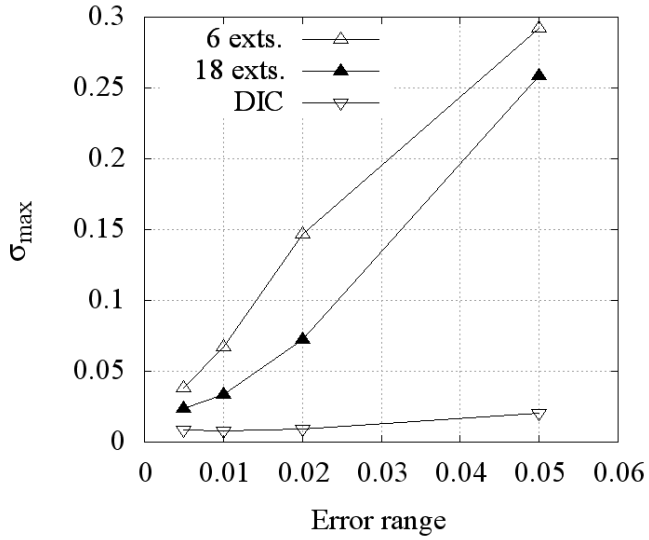


Figure 13. Comparison between different types of measurement

In general, more information is stored in the discrepancy function (i.e. more measurements are considered), more stable is the inverse problem even for high levels of errors. Thus the analysis using a continuous displacement field through DIC clearly outperforms the others in all error ranges. However, while the use of 6 extensometer provides acceptable results for k_N and k_V only for measurement errors associated with instrumentation precision of the 0.5% of the actual measured

displacement, good results can be obtained with 18 extensometer up to an error of 1% and with DIC up to an error of 5%.

7. Conclusions

In this work, an inverse method has been proposed for determining the elastic properties of an interface element, which can be used to model mortar joints in brick-masonry. A low-invasive in-situ experimental setup has been investigated, which consists of an in-situ test performed by utilising a vertical and a horizontal vertical flat-jack. Since the concern is about elastic properties, no information is needed about the existing state of stress, and only relative displacements due to flat-jacks loads have to be measured. A pseudo-experimental procedure has been followed, where sets of measurements have been generated numerically using a mesoscale FE model with known material parameters. Three different setups for the measurement instrumentation (in which respectively six extensometers, eighteen extensometers and the Digital Image Correlation procedure are utilised) have been considered, and in all cases the discrepancy between known and computed measures has been minimised using a Genetic Algorithm. Sensitivity and noise analysis have been performed to assess the stability of the procedure and the accuracy required by the experimental equipment. The comparison between the three setups shows that DIC outperforms the others as far as stability to measurement errors is concerned.
An experimental programme is planned to validate the proposed method, while future numerical research will focus on identifying inelastic properties of the same interface element for mortar joints.

Acknowledgements

This work has been partly supported by "FRA 2011" research funding of University of Trieste.

References

[1] P. Roca, M. Cervera, G. Gariup, L. Pela, Structural Analysis of Masonry Historical Constructions. Classical and Advanced Approaches, Arch. Comput. Methods Eng. 17 (2010) 299-325.
[2] P.B. Lourenço, Computational strategies for masonry structures, Ph.D. Thesis, Delft University Press, 1996.
[3] J.G. Rots (Ed), Structural Masonry: An Experimental/Numerical Basis for Practical Design Rules, A.A. Balkema, Rotterdam, 1997.
[4] P. Lourenço, J. Rots, J. Blaauwendraad, Continuum Model for Masonry: Parameter Estimation and Validation, J. Struct. Eng. 124(6) (1998), 642-652.
[5] P.B. Lourenço, J.G. Rots, Multisurface Interface Model for Analysis of Masonry Structures, J. Eng. Mech. 123 (1997), 660-668.

[6] L. Macorini, B.A. Izzuddin, A non-linear interface element for 3D mesoscale analysis of brick-masonry structures, Int. J. Numer. Meth. Engrg. 85 (2011), 1584-1608.
[7] L. Gambarotta, S. Lagomarsino, Damage models for the seismic response of brick masonry shear walls. Part I: the mortar joint model and its applications, Earthquake Eng. Struct. Dynam. 26 (1997),423-439.
[8] A. Brignola, S. Frumento, S. Lagomarsino, S. Podestà, Identification of shear parameters of masonry panels through the in-situ diagonal compression test, International Journal of Architectural Heritage: Conservation, Analysis, and Restoration 3 (2008), 52-73.
[9] K. Chaimoon, M.M. Attard, Modeling of unreinforced masonry walls under shear and compression, Eng. Struct. 29 (2007), 2056-2068.
[10] F. Da Porto, G. Guidi, E. Garbin, C. Modena, In-Plane Behavior of Clay Masonry Walls: Experimental Testing and Finite-Element Modelling, J. Struct. Eng. 136 (2010), 1379-1392.
[11] A. Tarantola, Inverse Problem Theory and Methods for Model Parameter Estimation, Society for Industrial and Applied Mathematics, Philadelphia, 2005.
[12] V. Buljak, Inverse Analyses with Model Reduction, Springer, Berlin, 2011.
[13] K. Danai, S.A. Civjan, M.M. Styckiewicz, Direct method of damage localization for civil structures via shape comparison of dynamic response measurements, Computers and Structures 92-93 (2012), 297-307.
[14] Z.R. Lu, J.K. Liu, Identification of both structural damages in bridge deck and vehicular parameters using measured dynamic responses, Computers and Structures 89 (2011), 1397-1405.
[15] L. Xu, B. Chen, Integrated vibration control and health monitoring of building structures using semi-active friction dampers: Part I-Methodology. Computers and Structures 30 (2008), 1789-1801.
[16] R. De-Carvalho, R.A.F. Valente, A. Andrade-Campos, Optimization strategies for non-linear material parameters identification in metal forming problems, Computers and Structures 89 (2011), 246-255.
[17] A. Orlowska, P. Kolakowski, J. Holnicki-Szulc, Modelling and identification of delamination in double-layer beams by the virtual distortion method, Computers and Structures 86 (2008), 2203-2214.
[18] M. Fontan, A. Ndiaye, D. Breysse, F. Bos, C. Fernandez, Soil-structure interaction: Parameters identification using particle swarm optimization, Computers and Structures 89 (2011), 1602-1614.
[19] J.H. Holland, Adaptation in natural and artificial systems, Ann Arbor, University of Michigan Press, 1975.
[20] D.E. Goldberg, Genetic algorithms in search, optimization and machine learning, Addison-Wesley, 1989. R. Fedele, G. Maier, M. Whelan, Stochastic calibration of local constitutive models through measurements at the macroscale in heterogeneous media, Comput. Methods Appl. Mech. Engrg. 195 (2006), 4971-4990.
[21] C. Chisari, L. Macorini, C. Amadio, B.A. Izzuddin, Identification of Brick-Masonry Material Properties Through Inverse Analysis and Genetic

Algorithms, in B.H.V. Topping, P. Iványi, (Editors), "Proceedings of the Fourteenth International Conference on Civil, Structural and Environmental Engineering Computing", Civil-Comp Press, Stirlingshire, UK, Paper 70, 2013. doi:10.4203/ccp.102.70.

[22] R. Fedele, G. Maier, M. Whelan, Stochastic calibration of local constitutive models through measurements at the macroscale in heterogeneous media, Comput. Methods Appl. Mech. Engrg. 195 (2006), 4971-4990.

[23] H. Diao, Y. Wei, On Frobenius normwise condition numbers for Moore-Penrose inverse and linear least-squares problems, Numer. Linear Algebra Appl. 14 (2007), 603-610.

[24] I. Rechenberg, Evolutionsstrategie: Optimierung technischer Systeme nach Prinzipien der biologischen Evolution, Frommann-Holzboog, 1973 (in German).

[25] S. Kirkpatrick, C.D. Gelatt Jr., M.P. Vecchi, Optimization by Simulated Annealing, Science 220 (1983), 671-680.

[26] A. Antonov, V.M. Saleev, An economic method of computing LP tau-sequence, USSR Computational Mathematics and Mathematical Physics 19 (1980), 252-256.

[27] J.E. Baker, Reducing Bias and Inefficiency in the Selection Algorithm, Proceedings of the Second International Conference on Genetic Algorithms and their Application, Hillsdale, New Jersey, (1987), 14-21.

[28] Z. Michalewicz, Genetic Algorithms + Data Structures = Evolution Programs, 3rd edition, Springer, Berlin, 1996.

[29] M. Srinivas, L.M. Patnaik. Genetic algorithms: A survey, IEEE Computer 27 (1994), 17-26.

[30] L. Binda, C. Tiraboschi, Flat-jack test as a slightly destructive technique for the diagnosis of brick and stone masonry structures, International Journal for Restoration of Buildings and Monuments (1999), pp. 449-472.

[31] I. Caliò, La prova di scorrimento con martinetto piatto, Proceedings of the Fourteenth Conference ANIDIS, Bari (Italy), (2011) (in Italian).

[32] R. Fedele, G. Maier, Flat-jack tests and inverse analysis for the identification of stress states and elastic properties in concrete dams, Meccanica 42 (2007), 387-402.

[33] B.A. Izzuddin, Nonlinear dynamic analysis of framed structures, Ph.D. Thesis, Department of Civil Engineering, Imperial College, London, 1991.

[34] C. Geuzaine, J.-F. Remacle, Gmsh: a three-dimensional finite element mesh generator with built-in pre- and post-processing facilities, Int. J. Numer. Meth. Engng. 79 (2009), 1309-1331.

[35] F. Hild, S. Roux, Digital Image Correlation: from Displacement Measurement to Identification of Elastic Properties - a Review, Strain 42 (2006), 69-80.